Structural Engineering and Mechanics, Vol. 4, No. 1 (1996) 9-23
DOI: http://dx.doi.org/10.12989/sem.1996.4.1.009

Dynamic response of elasto-plastic planar arches

S.L. Lee,† S. Swaddiwudhipong‡ and W.A.M. Alwis‡†

Department of Civil Engineering, National University of Singapore 10 Kent Ridge Crescent, Singapore 0511, Singapore

Abstract. The behaviour of elasto-plastic planar arches subjected to dynamic loads in presented. The governing equations are formulated through the dynamic equations and compatibility conditions. The latter is established by applying the generalized conjugate segment analogy. Bending moments at the nodes and axial forces in the members are considered as primary variables in the elastic regime. They are supplemented by the rotations at the nodes and dislocations in the elements when plastic hinges occur. Newmark-β method is adopted in the time marching process. The interaction diagram of each element is treated as the yield surface for the element and the associated flow rule is enforced as plastic flow occurs. The method provides good prediction of dynamic response of elasto-plastic arches while requiring small core storage and short computer time.

Key words: arches; dynamic response; elasto-plastic; plastic hinge; yield surface

1. Introduction

The response of structures to severe impulsive loadings involving both elastic and plastic regimes of the behaviour of materials is often required in the survivability design of buildings. An excellent guideline to the design of structures to blast loads was compiled and presented by the Task Committee on Updating Manual 42 of the ASCE Committee on Dynamic Effect of the Structural Division, (1985). Various aspects of nuclear weapon effects were discussed and simplified analysis of structures suitable for design purposes proposed.

In the earlier development of this subject, the elastic solution was first sought and correction applied when plastic hinge formed. Among others who adopted the abovementioned approach, Bleich and Salvadori (1955) proposed modified mode superposition method to study the impulsive motion of elasto-plastic beams while Berg and DeDeppo (1960) applied direct integration technique to solve the equations of motion of a structural system with masses lumping at the floor levels. The dynamic reponse of elasto-plastic beams was studied by Heidebrecht *et al.* (1963) using a discrete system approach. Tene *et al.* (1975) adopted backward differences in both space and time domains to solve the equations of motion governing the forced vibration of elastic arches. The effect of viscous damping was later considered by Sheinman (1979). Displacement components were chosen as primary variables in both of their studies. Lee *et al.* (1988) extended the discrete system approach to study the dynamic response of elasto-plastic frames and deep arches. Though the effect of axial force was considered in applying the yield surface, the effect of axial deformation was ignored and consequently the associated flow rule was not completely

† Professor
‡ Associate Professor
‡† Senior Lecturer

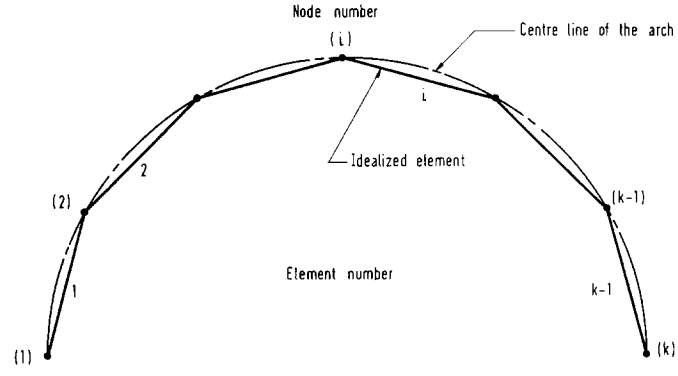

Fig. 1 Discretization of an arch

observed.

The present paper addresses the response of elasto-plastic arches under dynamic loads. The discrete system approach is adopted. The bending moments at the nodes and axial forces in the members are chosen as primary variables. They are supplemented by the rotation at the nodes, ϕ, and dislocation in the member, δ, when a plastic hinge forms. Once plastic flow occurs, the state of stress is carefully monitored and the associated flow rule is enforced. Direct time integration is carried out using Newmark-β method (Newmark 1959).

2. Structural idealization and assumptions

The structure is discretized into (k-1) straight elements connecting in a series at their nodal ends as shown in Fig. 1. The loadings, masses and damping effects are lumped and the plastic hinges are allowed to form only at the nodes. An elastic-perfectly plastic moment curvature relationship is assumed. Only loadings in the plane of the structure are considered in the study.

3. Equations of motion

The equations of motion are formulated through the virtual work principle and dynamic equilibrium conditions. For a structure with k nodes, there are k-3 independent mechanisms each comprising a segment of three consecutive elements as shown in Fig. 2. Applying the virtual work principle to each segment yields

$$-e_0M_i+e_1M_{i+1}-e_2M_{i+2}+e_3M_{i+3}=-a_{x1}Q_{x(i+1)}+a_{y1}Q_{y(i+1)}+a_{x2}Q_{x(i+2)}-a_{y2}Q_{y(i+2)} \tag{1}$$

where M_i, Q_{xi} and Q_{yi} are respectively the bending moment and D'Alembert forces in x and y directions and e_i, a_{xi} and a_{yi} are rotation and displacements in x and y directions at node i. The displacement components e_i, a_{xi} and a_{yi} are functions of coordinates at node i measured from any arbitrarily located origin.

Collecting the resulting k-3 equations leads to

$$[E]\ \{M\}=[A']\ \{Q\} \tag{2}$$

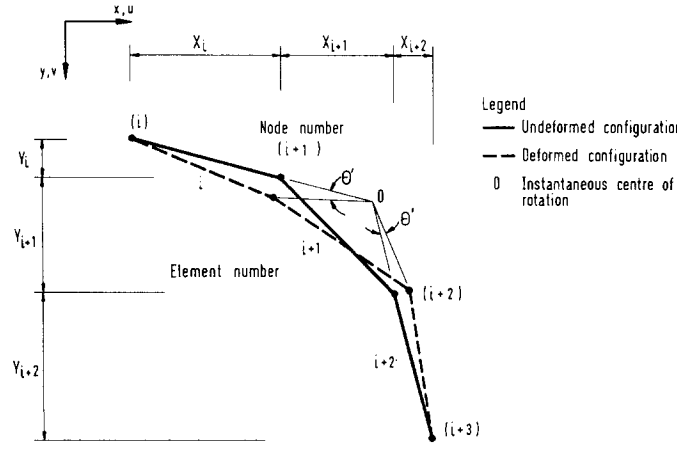

Fig. 2 A virtual displacement configuration for a three element segment

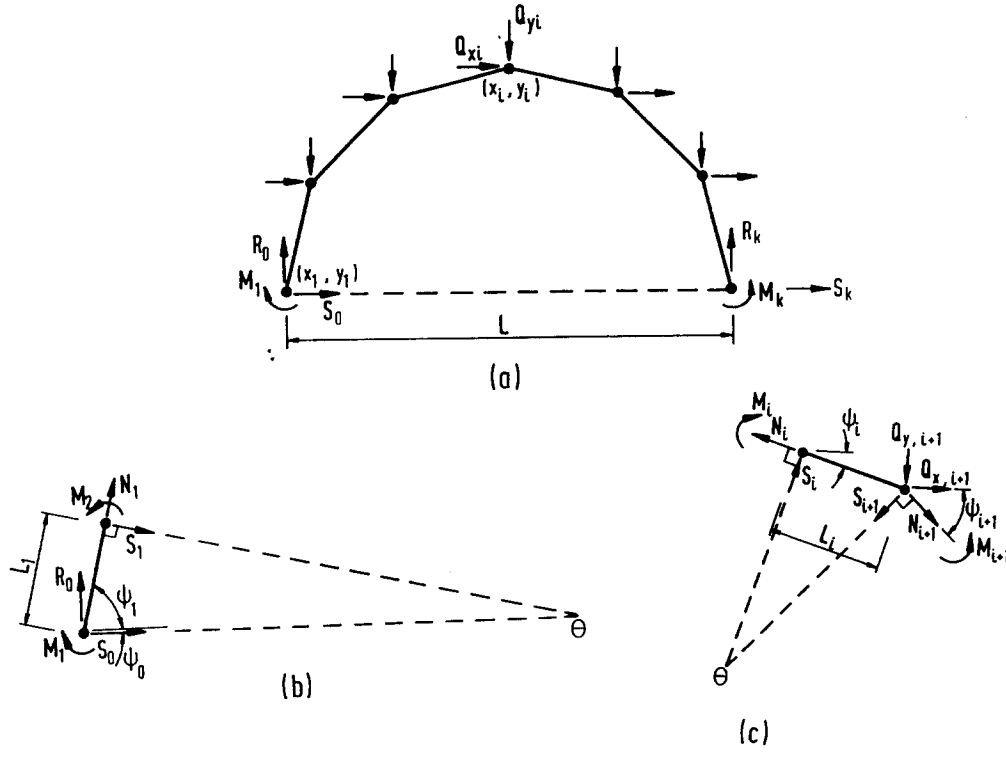

Fig. 3 Free body diagrams of (a) the entire arch, (b) the first element and (c) the i^{th} element

The D'Alembert force vector $\{Q\}$ is the vector of the resultants of the applied loads, the inertia forces and the damping resistance of the form

$$\{Q\}=\{p\}-[m]\{\ddot{u}\}-[c]\{\dot{u}\} \tag{3}$$

in which $\{p\}$ is the load vector, $\{u\}$ the displacement component vector, $[m]$ the mass matrix

and $[c]$ the damping matrix, superdot denoting differentiation with respect to time.

Considering the free body diagrams of the whole arch shown in Fig. 3a,

$$R_0 L=(M_n-M_1)+\sum_{i=2}^{k-1}[Q_{yi}(x_k-x_i)-Q_{xi}(y_k-y_i)] \tag{4}$$

Equilibrium of moment about θ in Fig. 3b gives

$$N_1=\frac{R_0 L}{L_1\sin(\psi_1+\psi_0)}+\frac{M_1-M_2}{L_1\tan(\psi_1+\psi_0)} \tag{5}$$

Free body diagram of element i provides

$$N_{i+1}=N_i\cos[\psi_i-\psi_{i+1}]-[M_{i+1}-M_i]\frac{\sin(\psi_i-\psi_{i+1})}{L_i}+Q_{x,i+1}\cos\psi_{i+1}-Q_{y,i+1}\sin\psi_{i+1} \tag{6}$$

Substituting Eq. (4) in Eq. (5) and assembling equilibrium equations of all (k-1) elements gives

$$\{N\}=-[G]\{M\}+[H]\{Q\} \tag{7}$$

in which $[G]$ and $[H]$ are functions of geometry of the structure and $\{N\}$ the axial force vector.

Substituting Eq. (3) in Eqs. (2) and (7) results in, respectively

$$\{A\}\{\ddot{u}\}+[C]\{\dot{u}\}+[E]\{M\}=\{D\} \tag{8}$$

and

$$[A_h]\{\ddot{u}\}+[C_h]\{\dot{u}\}+[G]\{M\}+\{N\}=\{q\} \tag{9}$$

where

$$[A]=[A'][m] \tag{10}$$
$$[C]=[A'][c] \tag{11}$$
$$\{D\}=[A']\{p\} \tag{12}$$
$$[A_h]=[H][m] \tag{13}$$
$$[C_h]=[H][c] \tag{14}$$
$$\{q\}=[H]\{p\} \tag{15}$$

4. Compatibility and displacement components

Compatibility conditions and displacement components are established through the conjugate segment analogy presented by Lee (1958) and generalized by Hjelmstad (1986). The constitutive relationship is taken into account in the formulation. A conjugate segment can be constructed such that it is identical with the actual structure but subjected to conjugate load and supported by conjugate shear forces and end moments. With the sign convention depicted in Fig. 4, it can be shown that the conjugate shear forces and concentrated loads are analogous to rotation in the actual segment, the conjugate distributed loads to the curvatures and the conjugate bending moments to the actual displacement components, and that the three compatibility equations for the actual segment can be derived through the application of the three independent equilibrium equations to the conjugate segment.

Equilibrium of forces on the conjugate segments depicted in Figs. 5(a) and 5(b) gives

$$\sum_{i=1}^{k} \varphi_i + \sum_{i=1}^{k-1} [\xi_{i-1} + \xi_i] M_i = 0 \tag{16}$$

$$\sum_{i=1}^{k} X_i \varphi_i + \sum_{i=1}^{k-1} \left[\xi_{i-1}\left(x_i - \frac{1}{3}X_{i-1}\right) + \xi_i\left(x_i + \frac{1}{3}X_i\right) \right] M_i$$

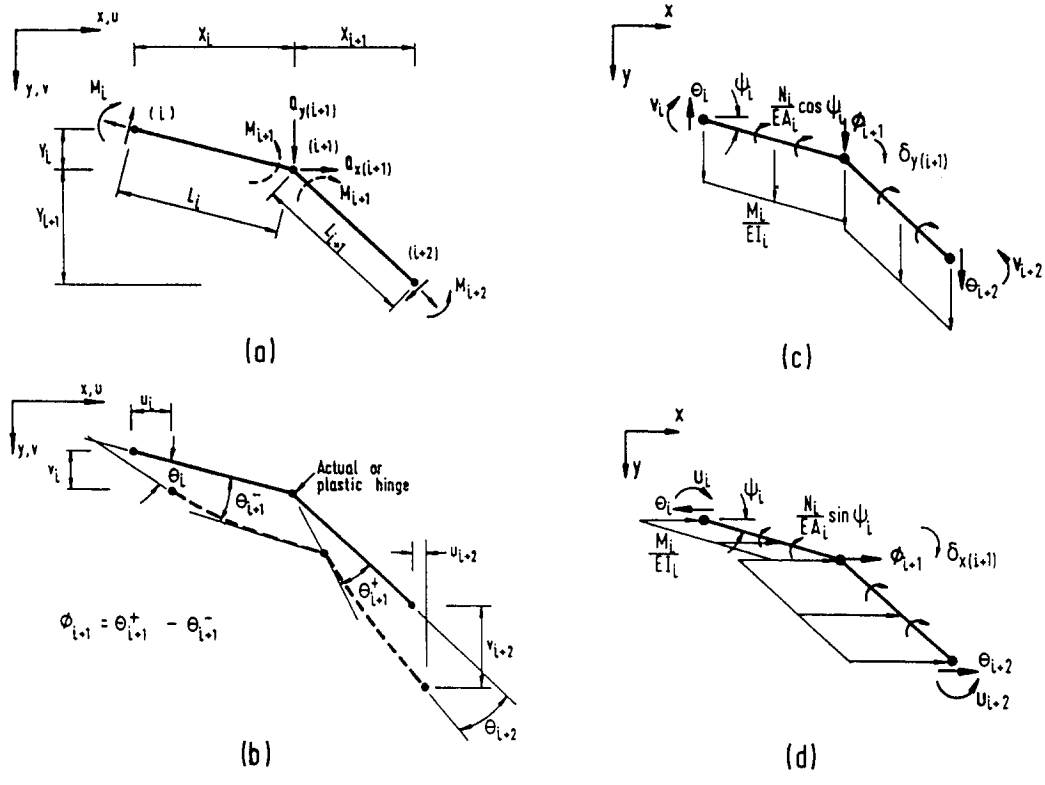

Fig. 4 Conjugate analogy (a) actions on actual structures, (b) displacement components, (c) conjugate segment for displacement v and (d) conjugate segment for displacement u

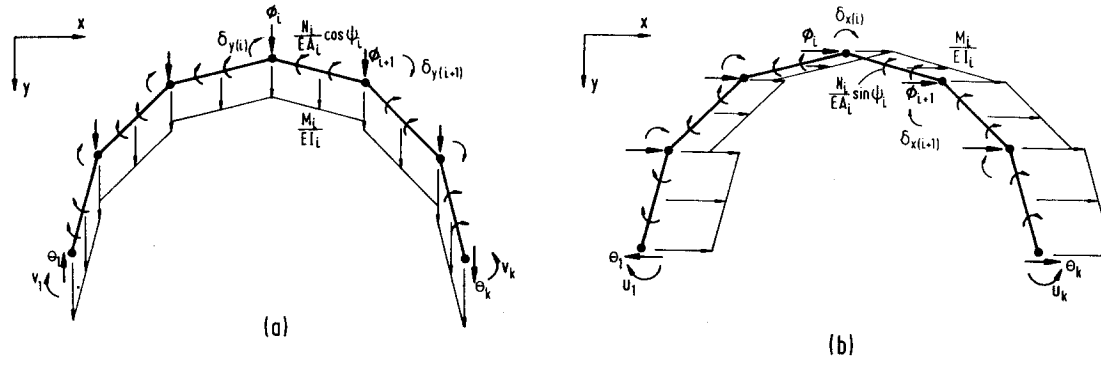

Fig. 5 Conjugate segments of the entire arch for (a) displacement v and (b) displacement u

$$+\sum_{i=1}^{k}\delta_{xi}+\sum_{i=1}^{k-1}\left[\frac{X_i}{E_iA_i}\right]N_i=0 \tag{17}$$

$$\sum_{i=1}^{k}y_i\varphi_i+\sum_{i=1}^{k-1}\left[\xi_{i-1}(y_i-\frac{1}{3}Y_{i-1})+\xi_i(y_i+\frac{1}{3}Y_i)\right]M_i$$
$$+\sum_{i=1}^{k}\delta_{yi}+\sum_{i=1}^{k-1}\left[\frac{Y_i}{E_iA_i}\right]N_i=0 \tag{18}$$

in which $\xi_i=\frac{1}{2}\frac{L_i}{EI_i}$ when $i=1, 2, \cdots, k\text{-}1$; $\xi_o=\xi_k=0$; δ_{xi} and δ_{yi} are dislocation components of node i in x and y directions respectively; X_i and Y_i are the projections of the length of element i, L_i, n x and y directions respectively.

Eqs. (16)-(18) can be written in collective form as

$$[K_\phi]\{\phi\}+[K_M]\{M\}+[K_\delta]\{\delta\}+[K_N]\{N\}=\{0\} \tag{19}$$

where $\{\phi\}$ is the actual or plastic hinge rotation vector, $\{\delta\}$ the dislocation vector, $[K_\phi]$, $[K_M]$, $[K_\delta]$ and $[K_N]$ are functions of geometry of the structure and the rigidity of the elements.

The bending moments in the conjugate segment represent the displacement components of the actual structure. Considering the conjugate segments shown in Fig. 6, the displacement components at node i of element i can be evaluated from

$$u_i=\sum_{j=i+1}^{k}(y_j-y_i)\varphi_j+\sum_{j=i+1}^{k}\left[(y_j-\frac{1}{3}Y_{j-1}-y_i)\xi_{j-1}+(y_j+\frac{1}{3}Y_j-y_i)\xi_j\right]M_j$$
$$+\frac{1}{3}Y_i\xi_iM_i+\sum_{j=i+1}^{k}\delta_{xj}+\sum_{j=i+1}^{k}\left[\frac{Y_j}{E_jA_j}\right]N_j \tag{20}$$

$$v_i=-\sum_{j=i+1}^{k}(x_j-x_i)\varphi_j+\sum_{j=i+1}^{k}\left[(x_j-\frac{1}{3}X_{j-1}-x_i)\xi_{j-1}+(x_j+\frac{1}{3}X_j-x_i)\xi_j\right]M_j$$
$$-\frac{1}{3}X_i\xi_iM_i+\sum_{j=i+1}^{k}\delta_{yj}+\sum_{j=i+1}^{k}\left[\frac{X_j}{E_jA_j}\right]N_j \tag{21}$$

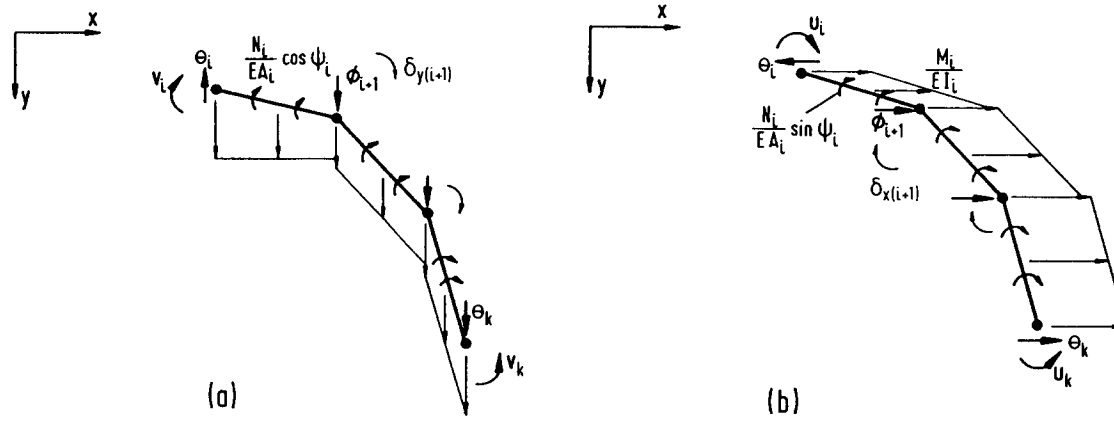

Fig. 6 Conjugate segments for (a) displacement v and (b) displacement u

which can be expressed collectively for all k nodes as

$$\{u\}=[G_\phi]\{\phi\}+[G_M]\{M\}+[G_\delta]\{\delta\}+[G_N]\{N\} \tag{22}$$

in which $[G_\phi]$, $[G_M]$, $[G_\delta]$ and $[G_N]$ are functions of geometry of the structure and the rigidity of the elements.

5. Time marching scheme

Discrete time integration is carried out using Newmark-β method (Newmark 1959). In the present study, the method comprises essentially the time discrete equations of motion, Eqs. (8) and (9), which can be expressed respectively at $(n+1)^{th}$ time step as

$$[Z_u]\{u_{n+1}\}+[E]\{M_{n+1}\}=\{D_{n+1}\}+[Z_u]\{x_n\}-[C]\{v_n\} \tag{23}$$

$$[Z_h]\{u_{n+1}\}+[G]\{M_{n+1}\}=\{N_{n+1}\}=\{q_{n+1}\}+[Z_h]\{x_n\}-[C_h]\{v_n\} \tag{24}$$

where

$$\{x_n\}=\{u_n\}+\tau\{\dot{u}_n\}+\tau^2\left[\frac{1}{2}-\beta\right]\{\ddot{u}_n\} \tag{25}$$

$$\{v_n\}=\{\dot{u}_n\}+\tau[1-\gamma]\{\ddot{u}_n\} \tag{26}$$

$$[Z_u]=\frac{1}{\beta\tau^2}[A]+\frac{\gamma}{\beta\tau}[C] \tag{27}$$

$$[Z_h]=\frac{1}{\beta\tau^2}[A_h]+\frac{\gamma}{\beta\tau}[C_h] \tag{28}$$

τ is the time step and β and γ the parameters defining the time marching scheme. The acceleration $\{\ddot{u}\}$ and velocity $\{\dot{u}\}$ at the $(n+1)^{th}$ time step are determined from

$$\{\ddot{u}_{n+1}\}=\frac{1}{\beta\tau^2}[\{u_{n+1}\}-\{x_n\}] \tag{29}$$

$$\{\dot{u}_{n+1}\}=\{v_n\}+\tau\gamma\{\ddot{u}_{n+1}\} \tag{30}$$

Compatibility equations, Eq. (19) and displacement components, Eq. (22) are enforced at each time step.

Equations of motion, Eqs. (23), (24) and the time discrete form of compatibility equations, Eq. (19), supplemented by Eq. (22) constitute the discretized form of governing equations to the problem.

6. Yield surface

The interaction diagram of each element, a typical of which is shown in Fig. 7, is adopted as the yield surface for that element. The diagram is a convex surface of the form

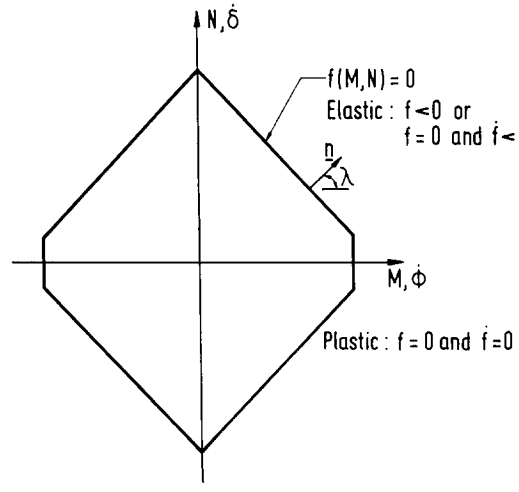

Fig. 7 A typical yield surface

$$f(M, N)=0 \tag{31}$$

The materials behave elastically if $f<0$ or $f=0$ and $\dot{f}<0$. Plastic flow occurs when $f=0$ and $\dot{f}=0$. The state of stress for which

$$f(M, N)>0 \tag{32}$$

is not permitted.

7. Actual and plastic hinges

If the structure is in the elastic regime and no actual hinge is present, all ϕ_i and δ_i vanish and M_i and N_i, the nodal bending moments and element axial forces are the unknown parameters to be determined. If an actual hinge exists at node j, M_j vanishes and ϕ_j the rotation at that node becomes the unknown variable. When plastic hinge forms just on the right of node l, the bending moment at that node and axial force in element l must satisfy the yield condition

$$f(M_l, N_l)=0 \tag{33}$$

and the associated flow rule

$$\dot{\delta}_l-\dot{\phi}_l \tan \Lambda_l=0 \tag{34}$$

where $\tan \Lambda_l$ is the slope of the outward normal to the yield surface at point (M_l, N_l).

The two extra unknowns, ϕ_l and δ_l introduced by the formation of plastic hinge just on the right of node l can be taken care of by the above two, Eqs. (33) and (34). If the corresponding yield point is at the corner of the yield surface, Eq. (34) is undefined but the values of M_l and N_l at that point are available from the diagram. The supplementary variables, ϕ_l and δ_l, are the only two new unknowns.

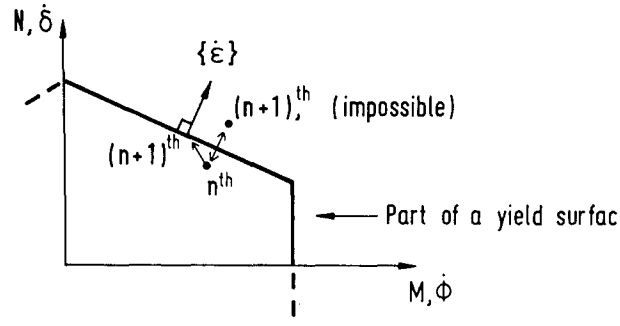

Fig. 8 Elasto-plastic phase change

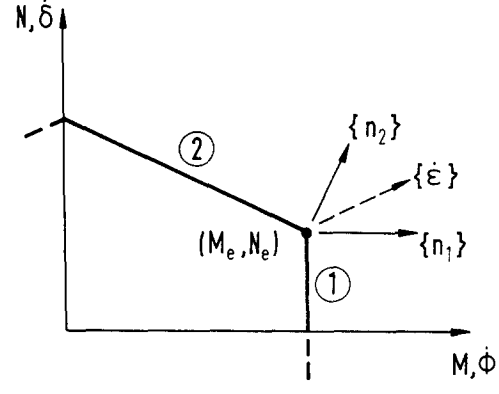

Fig. 9 Admissible strain rate vector at corner of yield surface

8. Transient phase changes

During the time marching process, the possibility of the phase change transitions, i.e. from elastic to plastic and vice versa is carefully monitored at each time step. If the results at the $(n+1)^{th}$ time step show that the state of stress is such that $f(M, N)>0$ which is impossible, the marching process is backtracked to the n^{th} time step and Eqs. (33) and (34) enforced as marching path on to the yield surface as illustrated schematically in Fig. 8. As plastic flow occurs, the direction of the strain rate vector, $\{\varepsilon\}^T=[\dot{\phi}\ \dot{\delta}]$ must satisfy the flow rule and is methodically handled. The violation of the associated flow rule, Eq. (34), signals a plastic-elastic transition. The marching is retreated by one step and the set of equations appropriate for elastic regime is reactivated. However, the permanent deformations ϕ_l and δ_l attained prior to the transition must be frozen and considered in the subsequent time steps.

When the yield point is at or in the neighbourhood of the corner of the yield surface, the monitoring of the stress path and the directon of the strain rate vector becomes more involved. The position of the yield point must be carefully traced and the appropriate marching scheme implemented accordingly. A special case arises when the yield point is at the corner where M_l and N_l become the known quantities but Eq. (34) is undefined. In this case, the strain rate vector must lie within the acute angle between or on the normal vectors to the two adjoining

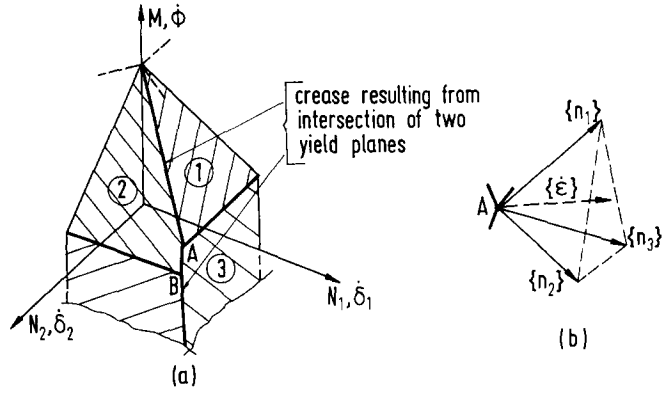

Fig. 10 A three dimensional stress space (a) yield surface and (b) admissible strain rate vector at corner A

yield planes, $\{n_1\}$ and $\{n_2\}$ as shown in Fig. 9. Mathematically, it should be possible to express

$$\{\dot{\varepsilon}\}=\lambda_1\{n_1\}+\lambda_2\{n_2\} \tag{35}$$

such that, λ_1 and λ_2 are both nonnegative real numbers. Inability to satisfy Eq. (35) indicates that the stress point starts to move away from the corner either along a yield plane ($\lambda_1=0$ or $\lambda_2=0$) or into the elastic domain ($\lambda_1<0$ and $\lambda_2<0$). The time marching scheme should be adjusted accordingly.

A more complicated case arises when the plastic hinges form either at both sides of a node or both ends of a member or combinations of both. Part of a typical three-dimensional stress space resulting from the composition of the two yield surfaces for the first case is shown in Fig. 10a. A similar yield surface in M_1-M_2-N space may be employed for the second and that of the multidimensional stress space for the combined case. As the yield point moves to the intersected corner of several planes *e.g.* point *A* or *B* in Fig. 10a, the direction of the strain rate vector is carefully traced and ensured to be on the surfaces of or within the polygonal pyramid surrounded by the normal vectors to all the yield planes meeting at that juncture. A typical admissible strain rate vector for point A of Fig. 10a is illustrated in Fig. 10b. If l yield planes meet at the corner, it should be possible to show that

$$\{\dot{\varepsilon}\}=\lambda_1\{n_1\}+\lambda_2\{n_2\}+\cdots\lambda_l\{n_l\} \tag{36}$$

while λ_i are all nonnegative real numbers. Violation of Eq. (36) implies the stress point moving away from the corner either along a crease or on a yield plane or into the elastic regime. The time marching scheme must be adjusted accordingly. Details on computational aspect of the method implemented in the programme are given in Lee *et al.* (1988b).

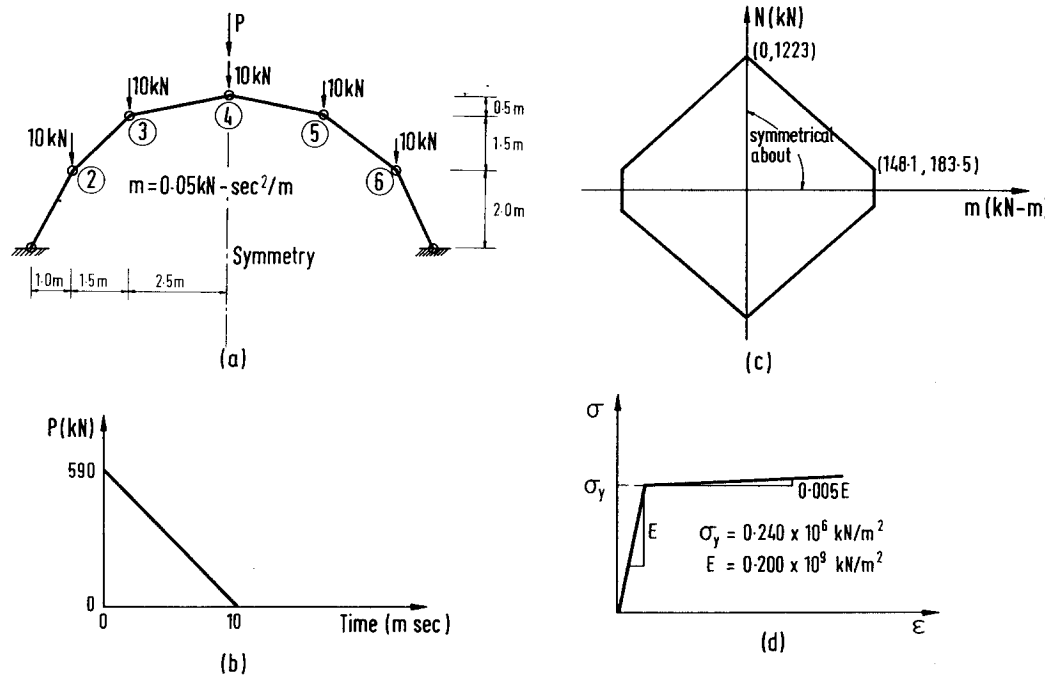

Fig. 11 Example 1 (a) model of steel arch (b) linearly decaying impact load, P (c) yield surface of each element and (d) material properties for finite element analysis

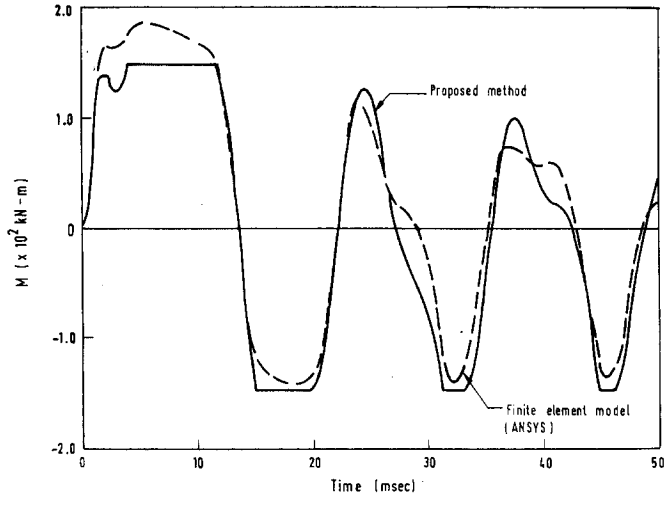

Fig. 12 Time history of the bending moment at node 4

9. Numerical examples

9.1. Example 1

A steel arch fabricated from six pieces of 305×165×40 kg/m Universal Beams as shown

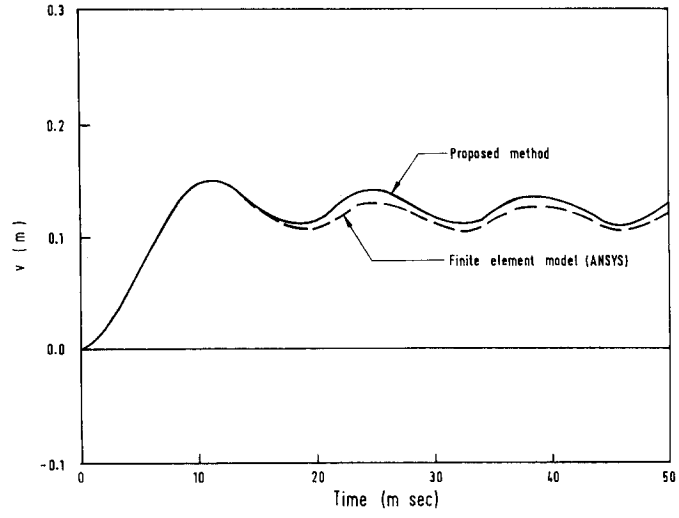

Fig. 13 Time history of the vertical deflection at node 4

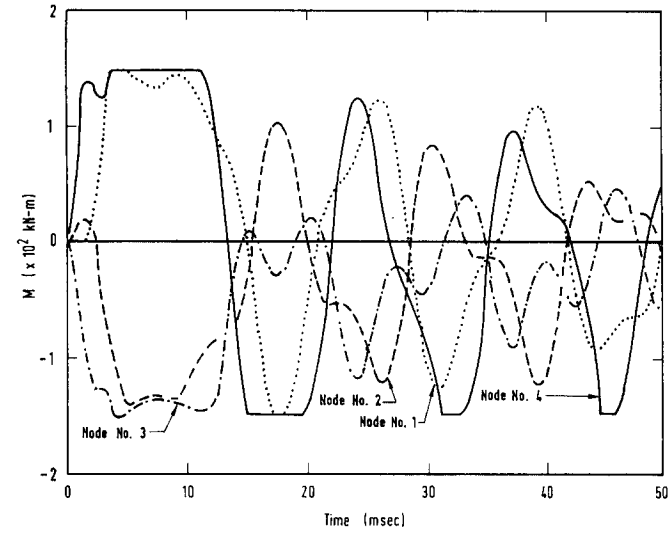

Fig. 14 Time histories of the bending moments at nodes 1 to 4

in Fig. 11a is analysed by the proposed method. The arch is subjected to a combination of dead load of 10 kN at each node and a triangular decaying vertical impact load at node 4. The variation and intensity of the impact load are illustrated in Fig. 11b. A lumped mass of 0.05 kN-sec^2/m is attached to each free node. An elastic-perfectly plastic moment-curvature relationship, the yield surface of which, is given in Fig. 11c is assumed in the present study.

The results from the analysis are compared with the finite element solutions obtained from the computer package "ANSYS". In the latter analysis, the elasto-plastic 2D beam element, STIF-23 is used to model the stiffness of the member while the lumped mass is represented by the general nodal mass element, STIF21. Material properties for the finite element analysis perfectly equivalent to the adopted yield surface shown in Fig. 11c are not available as perfectly plastic

Table 1 Details of blast load, Example 2

Node No	Arrival time ($\times 10^{-3}$ sec)	End time ($\times 10^{-3}$ sec)	Nodal forces at arrival time	
			Horizontal P_x(MN)	Vertical P_y(MN)
2	0	4	1.0	0.5
3	1	6	0.4	0.3
4	3	10	0.2	0.2
5	6	15	−0.1	0.1
6	10	30	−0.2	0.1

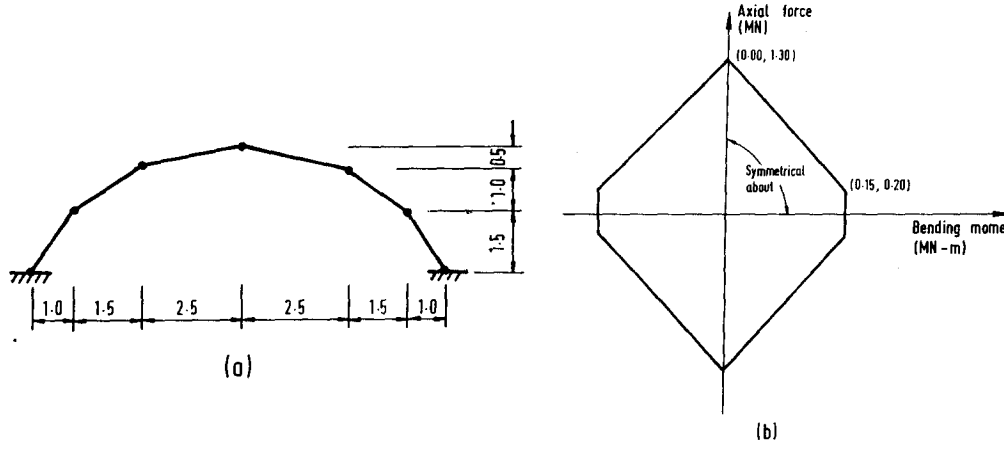

Fig. 15 Example 2 (a) geometry of the arch and (b) yield surface of each element

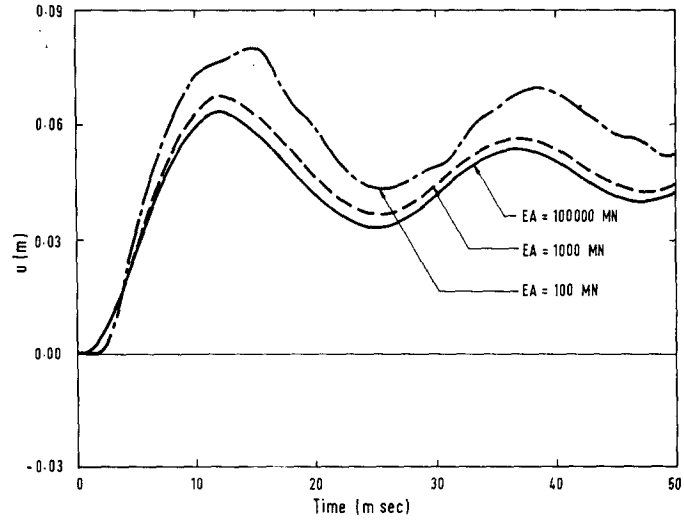

Fig. 16 Time history of lateral displacement at node 4

materials are not allowed in ANSYS and ii) elastic-perfectly plastic moment-curvature relationship is achieved only when the stress distribution over the whole section becomes at once fully plastic.

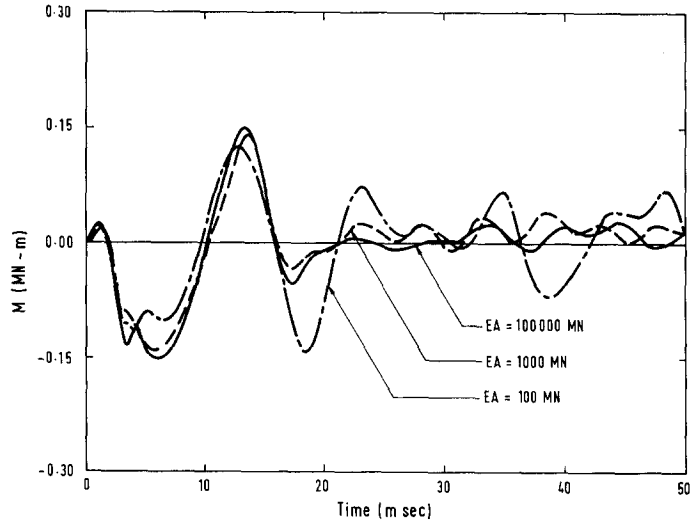

Fig. 17 Time history of bending moment at node 4

Closely equivalent material properties for the latter analysis adopted herein are given in Fig. 11d. The time step of 0.1 m sec is employed in both analyses.

Figs 12 and 13 show the time histories of the bending moment and the vertical deflection at node 4 resulting from both the proposed and finite element analyses. The results are well correlated. Minor differences in the variation of the bending moment especially at the earlier stage are most likely due to the discrepancies in the models for the material properties adopted in the two approaches as discussed earlier. The variation of bending moments at nodes 1 to 4 from the proposed analysis is shown in Fig. 14.

9.2. Example 2

The effects of axial deformation on the response of deep arches subject to dynamic loads are studied in the present example. The arch shown in Fig. 15a is subject to the blast loads, the details of which are given in Table 1. The flexural rigidity, EI, of each element is 17 MN-m^2 while the lump mass at each node is 0.05 MN-sec^2/m. The interaction diagram of each element is given in Fig. 15b. Various values of EA of 100, 1,000 and 10,000 MN for each element are considered.

The study based on a time step of 0.1 m.sec was carried out. The time histories of the horizontal displacement and bending moment at node 4 are illustrated in Figs. 16 and 17. The results show that the structures with less value of axial rigidity, EA, as expected deform larger than the stiffer ones. The formers have to resist more of the applied loads through their bending actions as demonstrated in Fig. 17.

10. Conclusions

The dynamic response of elasto-plastic planar arches is presented. The governing equations are formulated based on the equations of motion and supplemented by the compatibility condi-

tions established through the conjugate segment analogy. Since the bending moments at the nodes and axial forces in the members are chosen as primary variables, the monitoring of the stress path in and on the yield surface is direct, straight forward and more accurate. The state of stress at each time step is closely monitored while the associated flow rule is observed when plastic flow occurs. The time histories of the response of the arches are established using Newmark-β time marching scheme. The results obtained from the proposed method as compared with finite element solutions show reasonably good agreement. The structures with smaller values of axial rigidity have larger deflection and carry more loads through the bending actions. Small core storage and relatively very short computer time are required enabling the method to be easily implemented on small computer which is now available in most engineering offices.

References

ASCE Committee on Dynamics Effects of the Structural Division (1985), "Design of structures to resist nuclear weapons effects". *ASCE Manual and Reports on Engineering Practice* **42**.

Berg, G.V. and DeDeppo, D.A. (1960), "Dynamic analysis of elasto-plastic structures", *J. Eng. Mech., ASCE,* **86**, 35-58.

Bleich, H.H. and Salvadori, M.G. (1955), "Impulsive motion of elasto-plastic beam", *Transaction ASCE,* **120**, 499.

Heidebrecht, A.C., Fleming, J.F. and Lee, S.L. (1963), "Dynamic analysis of elastic multi-degree systems. *J. Eng. Mech., ASCE,* **89**, 190-215.

Hjelmstad, K.D. (1986), "Conjugate structure method", *J. Struct. Eng., ASCE,* **112**, 1413-1428.

Lee, S.L. (1958), "The conjugate frame method and its application in the elastic and plastic theories of structures", *J. Franklin Inst.,* **266**, 207-222.

Lee, S.L., Alwis, W.A.M., Swaddiwudhipong, S. and Mairantz, B. (1988a), "Elastoplastic dynamic analysis of plane frames and deep arches", *Int. J. Comp. Mech.,* **3**, 39-48.

Lee, S.L., Alwis, W.A.M., Swaddiwudhipong, S. and Mairantz, B. (1988b), "Computational aspect of dynamic analysis of elastoplastic arches", *Int. Series of Num. Math.,* **86**, 285-294.

Newmark, N.M. (1959), "A method of computation for structural dynamics", *J. Eng., Mech. ASCE,* **85**, 67-94.

Sheinman, I. (1979), "Forced vibration of a curved beam with viscous damping", *Comp & Struct.,* **10**, 499-503.

Tene, Y., Epstein, M. and Sheinman, I. (1975), "Dynamics of curved beams involving shear deformation", *Int. J. Solids Struct,* **19**, 827-840.